



Long-acting implantable dosage forms containing paliperidone palmitate obtained by 3D printing

Giuseppe Manini^{a,b,*}, Maud Deldime^a, Samira Benali^b, Jean-Marie Raquez^b, Jonathan Goole^a

^a Laboratory of Pharmaceutics and Biopharmaceutics, Université libre de Bruxelles, Campus de la Plaine, CP207, Boulevard du Triomphe, Brussels 1050, Belgium

^b Laboratory of Polymeric and Composite Materials (LPCM), Center of Innovation and Research in Materials and Polymers (CIRMAP), University of Mons, Place du Parc 23, B-7000 Mons, Belgium

ARTICLE INFO

Keywords:

Personalized medicine
Pressure extrusion-based printing
Paliperidone palmitate
Implantable dosage form
Cryogenic milling

ABSTRACT

In this work, the versatility of pressure extrusion-based printing (PEBP) was used as 3D printing process to create long-acting implantable dosage forms. Different release profiles were achieved based on the drug concentration, the way of preparation and the design of the final implants. Polycaprolactone (PCL) was used as the polymer to sustain the release of the loaded drug. Paliperidone palmitate (PP), a BCS Class II drug, used in the treatment of schizophrenia, was used as the model drug. Two PP concentrations (e.g. 5 and 10% w/w) as well as two methods of preparation before the 3D printing process, mortar and pestle and cryogenic milling, were evaluated. The amorphous state of PP was obtained by using cryogenic milling and it was maintained after printing. Two designs were printed by PEBP, a ring and a disk, to evaluate their impact on the release profile of PP. During the *in vitro* dissolution tests, the implant design, the amount of PP, as well as the crystalline or amorphous state of PP have shown to influence the drug release profile. During the successive steps of preparation of the long-acting implants, blends and raw materials were characterized by DSC and XRD.

1. Introduction

Nowadays, 3D printing no longer stops solely at the use of rapid prototyping. Indeed, pharmaceutical industry shows a growing interest towards this technique which allows the realization of tailored dosage forms (e.g. immediate release tablet (Pietrzak et al., 2015; El Aita et al., 2019), polypill (Khaled et al., 2015), implantable device (Holländer et al., 2016),...). Since early 90's, several printing techniques have been developed such as: powder-based printing (Infanger et al., August 2018), extrusion-based printing, stereolithographic printing (Xu et al., December 2019; Martinez et al., 2017), selective laser sintering (Fina et al., 2017; Fina et al., 2018) and inkjet printing (Cader et al., 2019; Sandler et al., 2011). Among these additive manufacturing techniques, three-dimensional (3D) printing, based on extrusion, remains the most widespread. As mentioned by Azad et al, between 2015 and 2019, the extrusion-based printing represented more than 80% of published

articles on 3D printing (Azad et al., 2020). Its ease of use, its versatility and its low cost make it one of the easiest techniques to be implemented, particularly Fused Deposition Modeling (FDM). In fact, FDM is a simple process based on the use of thermoplastic polymer in the form of filament, which is pushed through two gears in a heated barrel and extruded through a nozzle. The molten polymer is applied layer-by-layer to create the final product (Nober et al., 2019; Jonathan and Karim, 2015). Nevertheless, when used in pharmaceutics, FDM printing requires the preliminary preparation of drug-loaded filaments by a Hot-Melt Extrusion (HME) (Nober et al., 2019). To achieve a good printability, the polymer filaments must have the appropriate strength specificities to be rigid enough to get pushed by the printer gears as well as to be flexible enough to avoid any undesirable break during printing (Aho et al., 2016). In this respect, some excipients are often added to the polymer to act as plasticizer and decrease its processing temperature by lowering the melt viscosity (Aho et al., 2019). However, finding the

Abbreviations: CAD, Computer aided design; CM, Cryogenic milling; DDS, Drug delivery system; DSC, Differential scanning calorimetry; FDM, Fused deposition modeling; GPC, Gel permeation chromatography; HME, Hot-melt Extrusion; HSM, Hot stage microscopy; IVIVC, *in vitro in vivo* correlation; Mw, Molecular weight; PAM, Pressure-assisted microsyringe; PCL, Polycaprolactone; PEBP, Pressure extrusion-based printing; PM, Physical mixture; PP, Paliperidone palmitate; TGA, Thermogravimetric analysis; XRD, X-Ray diffraction.

* Corresponding author at: Laboratory of Pharmaceutics and Biopharmaceutics, Université libre de Bruxelles, Campus de la Plaine, CP207, Boulevard du Triomphe, Brussels 1050, Belgium.

E-mail address: giuseppe.manini@ulb.be (G. Manini).

<https://doi.org/10.1016/j.ijpharm.2021.120702>

Received 2 April 2021; Received in revised form 4 May 2021; Accepted 8 May 2021

Available online 12 May 2021

0378-5173/© 2021 Elsevier B.V. All rights reserved.

right strength properties to the filament is not straightforward as the number of excipients is limited to resolve this issue. Moreover, HME is considered as a stressful process as different degradation processes can occur during HME such as oxidation, hydrolysis, thermal or shear degradation. This is even bolstered during the process as any mechanical stress may induce further thermochemical degradation. Huang et al., studied the impact of different extrusion parameters such as the temperature, the residence time of the mixture inside the barrel or the screw design on HME process of gliclazide. They demonstrated that all these parameters had an impact on the stability of the drug and they have to be carefully determined to avoid any drug degradation (Huang et al., 2017). As alternative, FDM was also coupled with other automatic or manual process to fill hollow printed systems. During these processes, the printing was stopped, allowing the manual filling of the liquid formulation containing the drug. Then, the 3D printing was restarted to complete the printing of the caplet. However, these systems showed poor mechanical resistance and a lack of reproducibility (Melocchi et al., 2020).

To avoid an extrusion step and therefore to reduce the extent of thermal treatment, a pressure-based printing technique can be used as alternative. The thermoplastic polymer and the API are mixed beforehand and directly poured in a heated syringe. Then, the mixture is extruded through the nozzle by a pressured-air piston, mechanical force or by a screw (Azad et al., 2020). This technique was extensively used in the early 2000s, called as Pressure-Assisted Microsyringes (PAM), in tissue engineering to create soft tissue scaffolds (Jonathan and Karim, 2015). The interest of this technique is being grown since it does not require any post-production of filaments to obtain a printed formulation. Goyanes et al used a direct-powder printing process to create hydroxypropyl cellulose-itraconazole printlets directly from powdered materials without going through a filament production step (Goyanes et al., 2019).

To demonstrate the strength of this technique, paliperidone palmitate (PP), an atypical antipsychotic drug was selected as model to create 3D printed implantable dosage forms. It is a BCS class II drug with an extremely low solubility (below 0.1 µg/ml) (Remenar, 2014), a melting point around 115–117 °C (Leng et al., 2014) and sensitive to oxidation (Trivedi et al., 2013). Already marketed as long-acting injectable dosage form, this API is formulated as nanocrystal. After administration, the API slowly hydrolyzed to release palmitic acid and its active drug, the paliperidone (9-hydroxyrisperidone) (Leng et al., 2014). The use of nanocrystal enables to create controlled release dosage form where the dissolution profile is related to its proper solubility. However, leaving large amount of crystalline PP in the injection site may initiate a chronic granulomatous inflammatory reaction, as shown by Darville et al (Darville et al., 2014). In order to avoid this kind of reaction, the encapsulation or the dispersion of the drug into a polymeric matrix is considered (Elmowafy et al., 2020). By this way, its release profile will depend on the polymer chosen and not only on its solubility.

Polycaprolactone (PCL), a semi-crystalline polyester approved by The United States Food and Drug Administration, was used for its excellent biocompatibility and processability at low temperature (Holländer et al., 2016). This polymer is widely used in tissue engineering (Jiao et al., 2019; Park et al., 2016) and in the formulation of drug delivery systems (Holländer et al., 2016; Kempin et al., 2017). PCL degrades slower than usual other bioresorbable polymers, which makes it an excellent candidate for long-term drug delivery systems (DDS) (Sun et al., 2006). Selecting PCL to create DDS with an atypical antipsychotic drug has already been investigated in the literature. It has already been used to create implantable DDS of risperidone or paliperidone, which are parents molecules of PP. Yerragunta et al studied different molecular weight of PCL to obtain a 3-month release risperidone loaded-microspheres by o/w emulsion solvent evaporation technique (Yerragunta et al., 2015). Navitha et al, developed an implantable device based on different PCL molecular weight and Risperidone by HME. Their optimized implants released the drug *in vivo* for 3 months and they

achieved an *in vitro-in vivo correlation (IVIC)* (Navitha and Jogala, 2014).

Unfortunately, all these techniques did not allow the production of personalized dosage form.

In our study, a pressure-based printing technique was used to create PP-loaded implantable dosage forms. As the printing method does not have a proper mixing system, a preliminary mixing step must be carried out. Blends with different loadings of PP were prepared using two methods, the first with a mortar and a pestle and the second by cryogenic milling. This second method has the advantage of allowing to both finely disperse the API in the polymer matrix and the amorphization of the API. Then, the different blends were printed in 2 simple shapes, a solid disk and a ring to evaluate the impact of the design of the dosage form on the release profile of PP. In order to characterize thermal transitions of raw materials as well as the crystallinity and the amorphicity of the blends, DSC and XRD were used before and after printing.

2. Materials and experimental part

2.1. Materials

PCL 6500 (Mn 50,000 g/mol) was purchased as pellets from Solvay® (Belgium) and Paliperidone Palmitate was purchased from Biochem Partner® (China). Trifluoroacetic acid, tetrahydrofuran, acetonitrile and isopropanol were purchased from Sigma-Aldrich® (USA). Hydrochloric acid and Tween® 20 were purchased from VWR® (USA).

2.2. Methods

2.2.1. Preparation of the blends

Before preparing the blends with different loadings of PP, PCL pellets were crushed into powder using a cryogenic milling system (Retsch® Cryomill, Germany). The pellets were placed in a 25 ml stainless steel grinding jar with 3 stainless steel beads of 15 mm. The milling time was divided into 3 cycles of 2 min at 30 Hz, separated by cycles of 30 s at 5 Hz, to avoid any overheating. For each formulation, 10 g of a blend made of milled PCL and PP, was mixed using a mortar and pestle until no aggregates of drug or polymer were visually seen. The theoretical drug content was 5 or 10% w/w for each blend. Then, two of the four formulations were milled with the Cryomill® to evaluate the impact of a cryogenic milling on the amorphicity / crystallinity of the API (Table 1). The process was the same to that applied on PCL pellets.

2.2.2. Thermal analysis

Differential scanning calorimetry (DSC) analyses were conducted with a DSC Q2000 (TA Instruments®, New Castle, USA). Approximately 5–10 mg of samples were sealed in T_{zero} hermetic aluminum pan. The reference sample consisted of an empty pan. The samples were heated from –50 °C to 130 °C with a heating rate of 10 °C/min. The analyses were conducted under nitrogen atmosphere (50 ml/min).

Thermal decomposition of samples was assessed by thermogravimetric analysis (TGA). The analyses were performed with a TGA Q500 (TA Instruments®, New Castle, USA). The samples were heated from 30 °C to 450 °C with a heating rate of 10 °C/min.

2.2.3. Hot stage microscopy (HSM)

HSM was used to evaluate the printing temperatures of the different

Table 1
Compositions of the formulations.

Samples	PCL (%) w/w)	PP (%) w/w)	Cryogenic milling	Printing temperature (°C)
PCL_5PP_PM	95	5	No	100
PCL_5PP_CM	95	5	Yes	100
PCL_10PP_PM	90	10	No	110
PCL_10PP_CM	90	10	Yes	110

blends. The analyses were conducted on a BX 60 microscope (Olympus, Japan) equipped with a THMS600 hot stage (Linkham Scientific Instruments Ltd., Surry, England) and a TK-C1381 (JVC, Japan) video camera. 5 to 10 mg of samples were placed on a glass slide and fixed in the hot stage. The samples were heated from ambient temperature to 60 °C at a heating rate of 10 °C/min.

2.2.4. Gel permeation chromatography (GPC)

GPC analysis was conducted on an Agilent liquid Chromatography (Agilent Technologies®, United States) equipped with an Agilent degasser, an isocratic HPLC pump with a flow rate of 1 ml/min. Tetrahydrofuran was used as mobile phase and Polystyrene were used as standards for calibration. The GPC apparatus was equipped with an Agilent autosampler, the loop volume was 100 µL and the solutions were concentrated at 2 mg/ml. It was equipped with an Agilent DRI refractive index detector and three columns: a PL gel 5 mm guard column (Polymer Laboratories®, Ltd, United Kingdom) and two PL gel Mixed-B5µm columns (columns for separation of polystyrene with a Mw ranging from 200 to 4x10⁵ g/mol) were used at 30 °C to evaluate the Mw of samples.

2.2.5. Contact angle measurement

Contact angles were measured with a contact angle system OCA 15 from Dataphysics using the sessile drop technique. A sessile water droplet of 20 µL was deposited at the surface of the prepared sample by means of a syringe pump and the value of the contact angle was extracted from the recorded image of the droplet using a software based on the Laplace-Young model. Five droplets were deposited at different locations on the sample in order to obtain an average value.

2.2.6. X-ray diffraction (XRD)

X-ray diffractometer (D8 Advance Eco Bruker®, Madison, USA) equipped with a one-dimensional silicon detector (LynxEye, Bruker AXS) was used to characterize the crystalline/amorphous structure of powders, blends and implants. Using a Cu K α radiation (1.54 Å; 40 kV \times 25 mA) data were collected, over the angular range of 3–45° 2 θ and a step size of 0.02° and a dwell time of 1 s.

2.2.7. Determination of drug loading

To extract the PP, samples loaded with an average weight of 10 mg of API were solubilized in 1 part of acetonitrile under vortex until complete solubilization. Then, 9 parts of isopropanol were added drop by drop under vortex. Solutions were filtered through 0.45 µm filters (Sortorius®) and filled in 2 ml vial for HPLC analysis.

An HPLC-UV method was conducted to determine the drug loading from the extruded filaments as well as from the 3D devices.

Mobile phase A (100% v/v of acetonitrile) and mobile phase B (aqueous solution of trifluoroacetic acid at pH 2) were used at ratio 70/30 A/B (v/v). The flow rate was set at 1 ml/min for 20 min and the wavelength was fixed 278 nm. The retention time of PP was 8.0 min.

2.2.8. Design software

Tinkercad® was used as computer aided design (CAD) program to draw the implantable dosage forms and export them as .stl files to the 3D printer. A ring and a disk were the two shapes that were investigated to compare the influence of the design on the dissolution profile of the loaded PP.

The dimensions of the rings and the disks that were used in this work as potential implantable dosage forms are shown in Fig. 1. The thickness of both implants was 1.2 mm, the diameter of the disk was 25 mm and the external/internal diameters of the ring were 30 mm/25 mm, respectively. The calculated surface and volumes of these models were 592 mm² & 229 mm³ and 1059 mm² and 579 mm³ for the ring and for the disk, respectively. The surface to volume ratios were 2.6 and 1.8 mm²/mm³ for the ring and the disk, respectively.

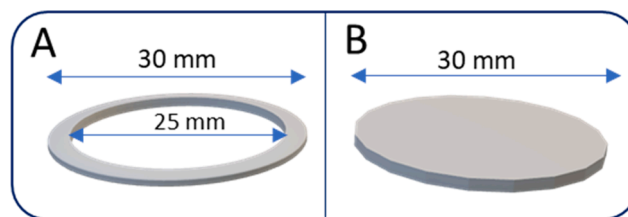


Fig. 1. Representation and dimensions of the ring (A) and the disk (B) used as implantable dosage forms.

2.2.9. 3D printing

A Hyrel® System 30 M (Atlanta, USA) was used as 3D printer with a specific VOL-25 printhead and a nozzle diameter of 1.3 mm. The Syringe was filled with the formulation and pre-heated to the define printing temperature till total melting. The build plate was heated to 40 °C, the printing speed set at 10 mm/sec and the flow rate at 5.0.

2.2.10. Dissolution test

The dissolution tests were performed in a GFL® (Burgwedel, Germany) water bath kept at 37 °C. The dissolution medium was adapted from the guidance published by the Food and Drug Administration (Dissolution Database of the API (Dissolution Methods Database, 2021) and contained 2% (w/w) of Tween® 20 in 0.001 N HCl. Implants from PCL_5PP_{PM} & PCL_5PP_{CM} were placed in 20 ml of dissolution medium while implants from PCL_10PP_{PM} & PCL_10PP_{CM} were placed in 40 ml of dissolution media. The dissolution medium was completely changed every sampling time to preserve sink condition.

3. Results and discussion

3.1. Characterization of the starting materials

In order to evaluate the thermal stability of the materials before 3D printing process, thermal characterization using TGA were conducted on starting materials, i.e., PCL and PP. During the analysis, the percentage of weight loss and its first derivative were plotted in Fig. 2.

The percentage of weight loss and its first derivative did not show any residual moisture or weight loss evolved until 200 °C, indicating that both starting materials will be stable enough to undergo heat treatment. To further support this thermal analysis, HPLC was also used to evaluate any potential thermochemical instability of PP and PCL after 3D printing (Table 2).

In addition to the evaluation of the stability temperature, it was required to evaluate the extrusion/printing temperatures to be considered for these different blends. DSC analyses were thereby conducted on the starting materials to highlight the different thermal transitions occurring during a heating cycle for each product as well as to determine the range of printing temperature (Fig. 3).

In accordance with the data already published in the literature, PCL showed a relatively wide melting range with a maximal endothermic peak at 61 °C (Holländer et al., 2016). For PP, a melting point was found at 115 °C (Leng et al., 2014). Since PCL was characterized by a relatively low melting point, the melting point of PP can be considered as decisive for the printing process. Indeed, if PEBP is performed at a temperature that is not sufficient to melt the drug, it may block the materials at the nozzle and stop the process.

To confirm the amorphization, we performed the XRD analyses on both products to evaluate the specific crystalline structure of PP and PCL before 3D-printing (Fig. 4).

In accordance with the data already published in literature, PP showed two major peaks at 5.1° and 7.7°, corresponding to the crystalline state of PP (Leng et al., 2014). On the other hand, the semi-crystalline polymer, PCL, showed two Bragg peaks at 21.4° and 23.8° (Holländer et al., 2016; Li et al., 2010; Cheng et al., 2009), which is

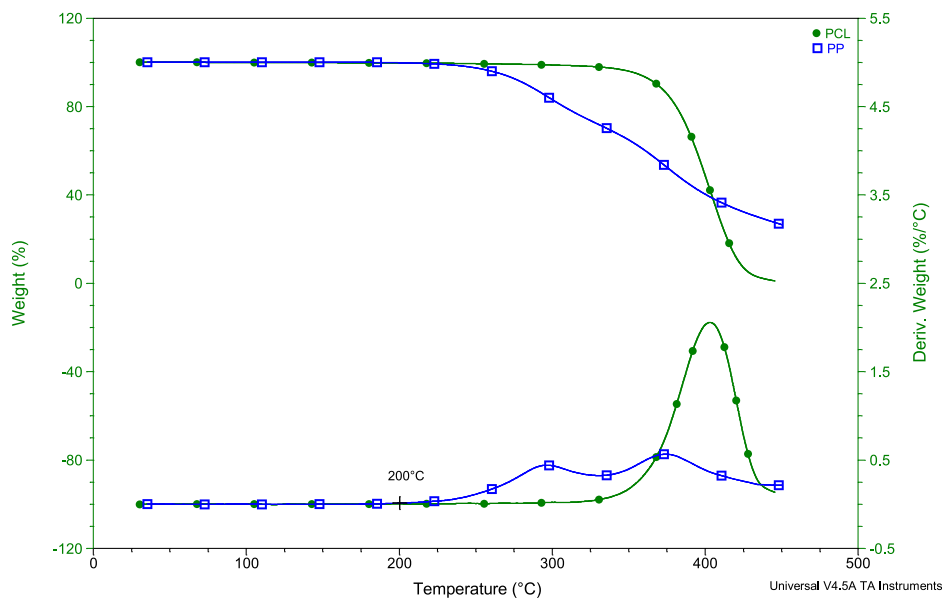


Fig. 2. TGA results for PCL (green curve), PP (blue curve).

Table 2

The average weight (\pm SD, $n = 3$) by printed shape and the average % of PP measured by HPLC (\pm SD, $n = 3$).

Blends	Shape	Weight \pm SD (mg)	% of paliperidone palmitate
PCL_5PP_PM	Ring	280.4 \pm 9.9	4.58 \pm 0.03
	Disk	621.2 \pm 29.8	
PCL_5PP_CM	Ring	283.9 \pm 14.8	4.45 \pm 0.27
	Disk	629.6 \pm 23.1	
PCL_10PP_PM	Ring	307.3 \pm 0.9	9.29 \pm 0.17
	Disk	649.3 \pm 34.8	
PCL_10PP_CM	Ring	302.0 \pm 2.5	10.10 \pm 0.15
	Disk	630.1 \pm 32.2	

ascribed to the characteristic diffraction peaks of crystallographic lattices for PCL. Since the polymer does not show any peaks between 4° and 8° , the presence or absence of both major PP peaks could be used as a way to attest for the crystalline state of PP in the blends and the 3D-

printed dosage forms.

3.2. Characterization of blends

After the thermal characterization of our starting materials, two blends containing 5 and 10% w/w of PP were prepared before the PEBP process using a mortar and a pestle. Then, two blends containing 5 and 10% w/w of PP were cryogenically milled. In order to differentiate the different methods of preparation, the blends having been mixed by mortar and pestle were named "PM" and those having undergone cryogenic milling, "CM".

The blends prepared by mortar and a pestle showed a melting endotherm respectively at 97°C and 106°C (Fig. 5). These melting points, corresponding to PP, appeared at a temperature lower than the initial melting point of PP, which was found to be 115°C . During this study, the solubilization of PP within PCL was observed and correlated with the decrease in melting point of PP obtained by DSC. Such decrease

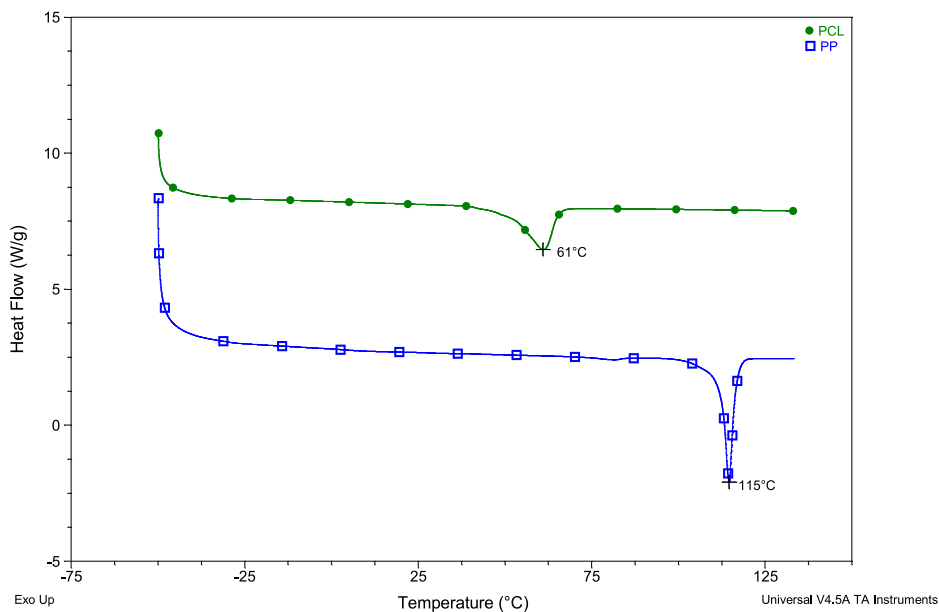


Fig. 3. DSC results of raw materials, PCL (green curve), PP (blue curve).

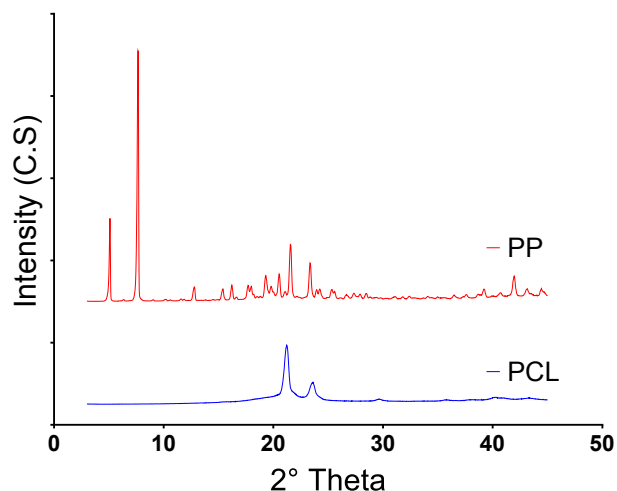


Fig. 4. X-Ray Powder Diffractogram of PCL (blue curve) and Paliperidone Palmitate (red curve).

may appear when the API solubilizes within the polymer during a heating cycle. Indeed, Marsac *et al.* have shown that miscible drug-polymer mixtures may show a decrease of the melting point of the drug, while immiscible or partially miscible systems do not present such a depression in terms of melting point (Marsac *et al.*, 2009). Regarding the melting enthalpy of PCL_5PP_{PM} & PCL_10PP_{PM} at 97 °C and 106 °C, showed a melting enthalpy of 1.2 and 4.0 J/g, respectively. Based on the drug content of each formulation and the sample weight, the normalized crystallinity of PP in the physical mixtures was 21% and 35% for PCL_5PP_{PM} & PCL_10PP_{PM}.

In contrast, cryogenically milled blends containing 5 and 10% w/w of PP do not present any melting point other than the polymer. This lack of melting point may be explained by the PP amorphization obtained during the preparation of these blends. During the milling step, the mechanical energy was transferred to the drug, which led to accumulation of defects and disrupted its crystal structure (Loh *et al.*, 2014). In addition to the DSC, an XRD analysis was performed on the same blends.

As previously mentioned, the crystalline structure of PP may be observed by the presence of two characteristic peaks at 5.1° and 7.1°. The blends prepared by mortar and a pestle contained both

characteristic peaks of PP and another one at 16.2°, which also belonged to the drug (Fig. 6), whereas these peaks were not present in blends prepared by cryogenic milling. It can also be noted that the PCL pattern remains unchanged for all blends, regardless of the preparation way.

The PEBP temperatures of the blends were determined using DSC results. Since the melting point of PP was shown at 97 °C for PCL_5PP_{PM} blend, the temperature at 100 °C was selected as the minimal printing temperature. This allowed the melting of both polymer and API. In addition, as PCL_5PP_{CM} blend contained the same amount of drug, a temperature of 100 °C was also used. For the blend containing 10% w/w of PP prepared by mortar and a pestle, DSC curve showed a melting point at 106 °C. This let us to set the minimum extrusion and printing temperature at 110 °C. This printing temperature was also used for PCL_10PP_{CM} as it contains the same amount of PP as PCL_10PP_{PM}. Compared to the TGA results, no weight loss was observed for the polymer and PP under 100 °C or 110 °C (Fig. 2). Moreover, these temperatures are in relationship with those found in the literature for printing PCL (Holländer *et al.*, 2016; Yang *et al.*, 2018).

3.3. Implants printing

The PEBP process was performed with the Hyrel® System 30 M as 3D printer, which was equipped with a VOL 25 modular head (Fig. 7). The mixture was filled into the reservoir, heated and then printed following the .gcode file. However, prior to the printing, the blend must be

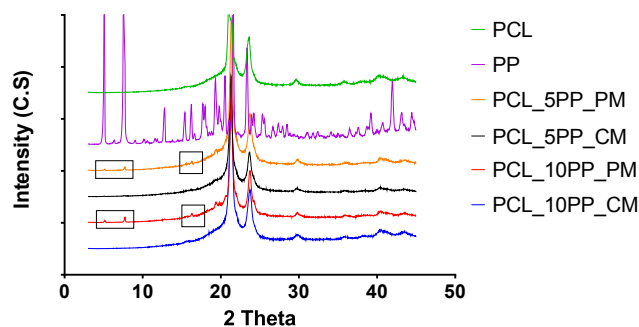


Fig. 6. XRD results of different blends after physical mixture (PM) or cryogenic milling (CM).

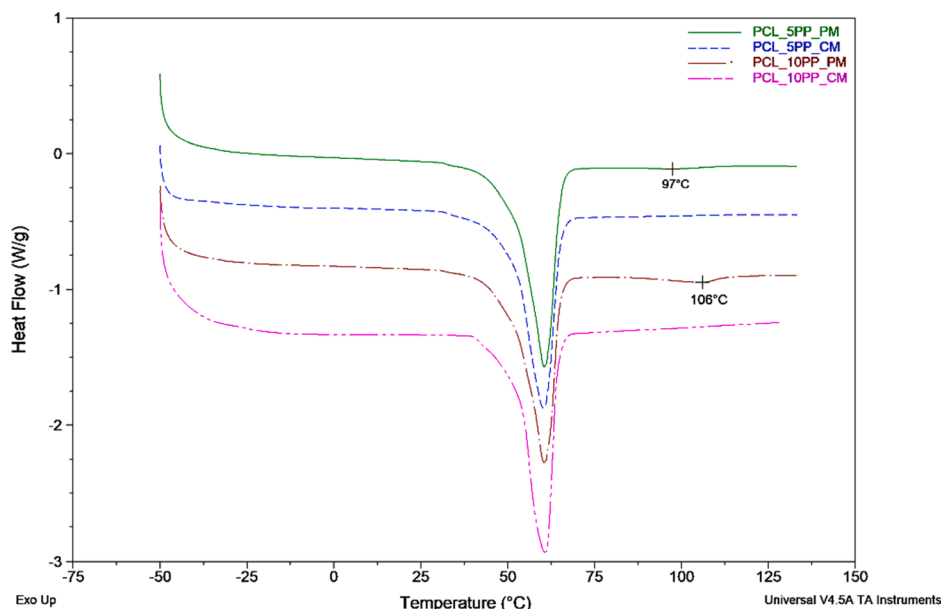


Fig. 5. DSC results of different blends after physical mixture (PM) or cryogenic milling (CM).

properly homogenized as the VOL 25 modular head was not equipped with a mixing system. The homogeneity of the blend was assessed at the end of the process, on the 3D printed implants (HPLC results, Table 2). The blend was heated at the determined temperature for 10 min before the printing process to allow the complete melting of the formulation. Then, the syringe was upside down turned and the printing could resume. For each blend, two designs were printed, i.e., a ring and a disk (n = 3), which was previously designed with Tinkercad™ (Fig. 7).

A printing speed of 10 mm/s was set and the building plate was heated at 40 °C to ensure a good adhesion of the dosage forms during the printing.

Using these printing parameters, as well as the temperatures determined by DSC, i.e., at 100 °C for blends containing 5% w/w of PP and at 110 °C for blends loaded with 10% w/w of PP, no blockage at the printing head was observed during the process. After printing, in addition to quantification of PP, the dosage forms were weighed to evaluate the reproducibility of the process (Table 2).

However, the use of PEBP as 3D printing technique involved a potential thermal stress, which may degrade the drug during the process. Such degradation cannot be evaluated by the uniformity of weight. Therefore, PP was extracted from the implants by a liquid-liquid extraction method and characterized by HPLC.

As it can be seen, the standard deviations of the weighted printed implants remained relatively low (Table 2). Such results were encouraging as a poor mass uniformity is known to lead to different amounts of drug in the final dosage forms and can therefore have an impact on its release profile.

The HPLC results obtained after extraction of the drug have showed a percentage of 4.58% and 4.45% for blends PCL_5PP_{PM} and PCL_5PP_{CM}, respectively. The percentage of loaded PP from blends PCL_10PP_{PM} and

PCL_10PP_{CM} were found to be 9.29% and 10.10%, respectively. These results were closed to the expected theoretical values, which were 5% w/w from PCL_5PP_{PM} and PCL_5PP_{CM} and 10% w/w from PCL_10PP_{PM} and PCL_10PP_{CM}. The chromatographs did not show any degradation products of PP.

3.4. Characterization of implants

In addition to the PP quantification after the printing process, its crystallinity/amorphization must be evaluated as well. For that reason, DSC analysis after PEBP was interesting to evaluate any potential presence of PP crystals after printing. In addition, it was used to assess if the amorphization obtained after cryogenic milling was maintained after a thermal process.

DSC results showed very small endothermic peaks at 83 °C for PCL_5PP_{PM} 3D and at 90 °C for PCL_10PP_{PM} 3D (Fig. 8). Those temperatures were lower than those observed from the physical mixtures which were 97 °C and 106 °C from PCL_5PP_{PM} and PCL_10PP_{PM}, respectively (Fig. 5). After 3D printing, the crystallinity of PP in PCL_5PP_{PM} and PCL_10PP_{PM}, based on the melting enthalpy, remained 6% and 17% respectively. Indeed, heating above its melting temperature and the rapid cooling of the material after extrusion through the nozzle of the printer resulted in the partial amorphization of the drug. In this case, the amorphization was partial, as residual crystals were present after the process. Nevertheless, PCL_5PP_{CM} and PCL_10PP_{CM} did not show another melting point than that corresponding to PCL. Therefore, it could be concluded that cryogenic milling allowed maintaining the amorphous state of PP after a 3D printing step.

In addition, XRD showed the absence of characteristic peaks at 5.1 and 7.1° of the crystalline state of PP for PCL_5PP_{CM} and PCL_10PP_{CM} after 3D printing (Fig. 9). For the other blends, which were prepared with a mortar and a pestle, both characteristic peaks remained present. Nevertheless, there could be a slight decrease in crystallinity as the peak as previously observed at 16.2° was not found herein. Such observation confirmed a partial amorphization of PP from blends A and C as well as the preservation of its amorphous state from PCL_5PP_{CM} and PCL_10PP_{CM}.

Moreover, the crystalline residues that were present in PCL_5PP_{PM} and PCL_10PP_{PM} could be visually observed by using a hot stage polarized microscope. Indeed, from 60 °C, the polymer was in the molten state and only PP crystals remained in the solid state. Using polarized glass, any light-diffracting residues could be seen (Fig. 10).

As it can be observed, large crystals and agglomerates of PP were still present in the 3D printed dosage forms from PCL_5PP_{PM} and PCL_10PP_{PM} (Fig. 10B and 10F). These were also visible with the use of a polarized glass (Fig. 10A and 10E).

In contrast, no crystalline structure was noticed in the 3D printed dosage forms from PCL_5PP_{CM} and PCL_10PP_{CM}. The use of cryogenic milling avoided the presence of crystalline residues after PEBP (Fig. 10C, D, G and H).

3.5. In vitro drug release from 3D printed implants

In order to evaluate the PP percentage that can be released from the 3D-printed implants, a dissolution test was performed. The different 3D-printed dosage forms were placed in the dissolution media adapted from the FDA dissolution database (Dissolution Methods Database, 2021) and placed in a heated bath at 37 °C with a constant horizontal shaking fixed at 50 RPM. The dissolution medium were completely replaced at different periods of time and analyzed by HPLC to quantify the amount of PP that was released.

Fig. 11 represents the cumulative percentage of PP released over time from implants made with blends PCL_5PP_{PM} & PCL_5PP_{CM} which were loaded with 5% w/w PP (Fig. 11, I) and with blends PCL_10PP_{PM} & PCL_10PP_{CM} which loaded with 10% w/w of PP (Fig. 11, II).

Rings and disks printed from PCL_5PP_{PM} (Fig. 11, I) had an initial

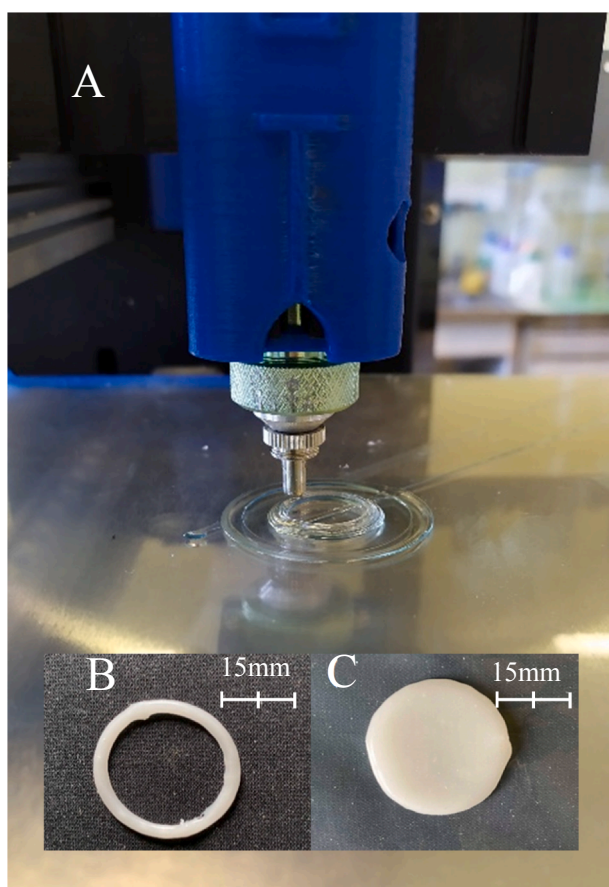


Fig. 7. 3D printing of an implant on the Hyrel System 30 M (a), 3D printed ring shape (b) and 3D printed Disk shape (c).

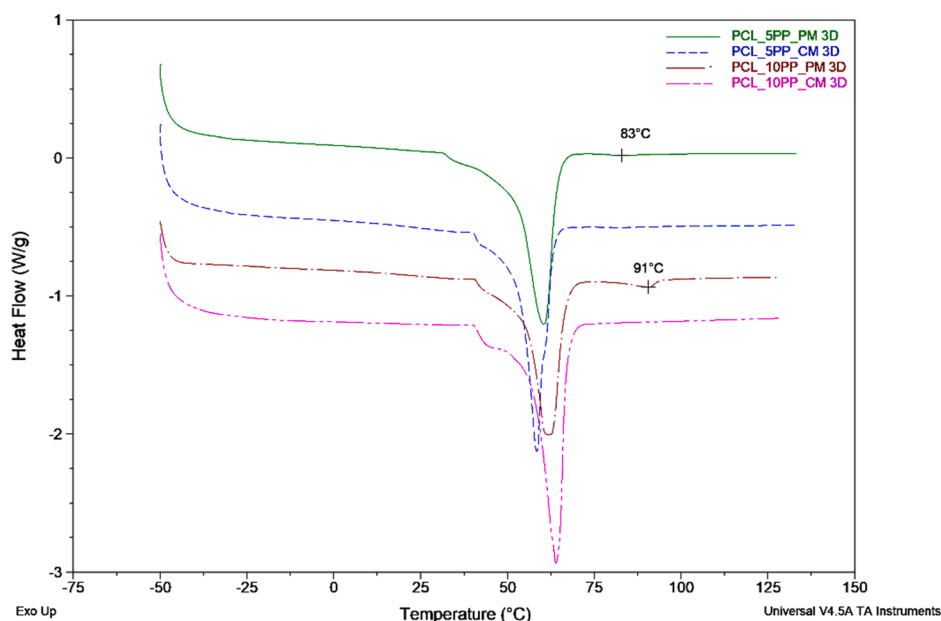


Fig. 8. DSC results of the different blends after 3D printing.

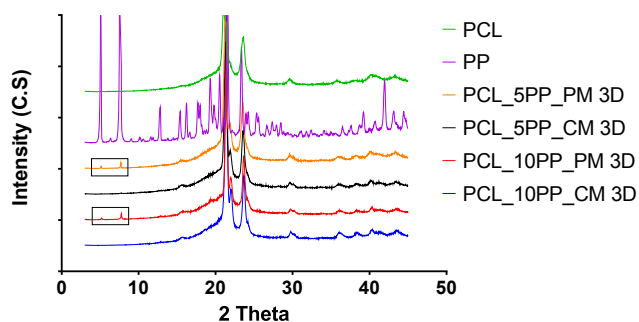


Fig. 9. XRD results of raw PCL, PP and the different blends after 3D printing.

release of $25.6 \pm 2.4\%$ and $16.1 \pm 0.9\%$ of PP after 1 day, respectively. For PCL_5PP_CM (Fig. 11, I), the rings and disks released $20 \pm 0.3\%$ and $14.3 \pm 1.2\%$ of PP after 1 day. From the outset, a lower percentage of PP was released from the disks than rings independently of the blend. However, implants printed from PCL_5PP_PM showed a slightly higher

percentage of drug released after 1 day. After 3 months, rings and disks printed with PCL_5PP_PM released $79 \pm 3\%$ and $63 \pm 3\%$ w/w of PP, respectively.

At the same time, implants printed from PCL_5PP_CM released $67.7 \pm 0.4\%$ and $57.8 \pm 3.6\%$ w/w of PP for the rings and disks. Even after 3 months, the difference in the percentage of PP released remained similar. Indeed, a higher percentage of PP was released from the rings compared to the disks. In terms of preparation way, the amorphous state of PP in PCL_5PP_CM did not accelerate the release of the drug. However, the design of the printed object had the major impact on the release profile of the drug.

On the other side, rings and disks printed with PCL_10PP_PM (Fig. 11, II) released $14.1 \pm 0.5\%$ and $7.8 \pm 1.2\%$ of PP after 1 day. While the initial released for rings and disks printed with PCL_10PP_CM showed equivalent drug released than PCL_10PP_PM. For formulations loaded with 10% of PP, the highest percentage of PP that was released was achieved by the rings. In this case, both formulations released the same drug percentage after 1 day unlike blends loaded with 5% w/w of PP. From the first day, the release profiles between the rings and disks printed with PCL_10PP_PM and PCL_10PP_CM were almost identical until

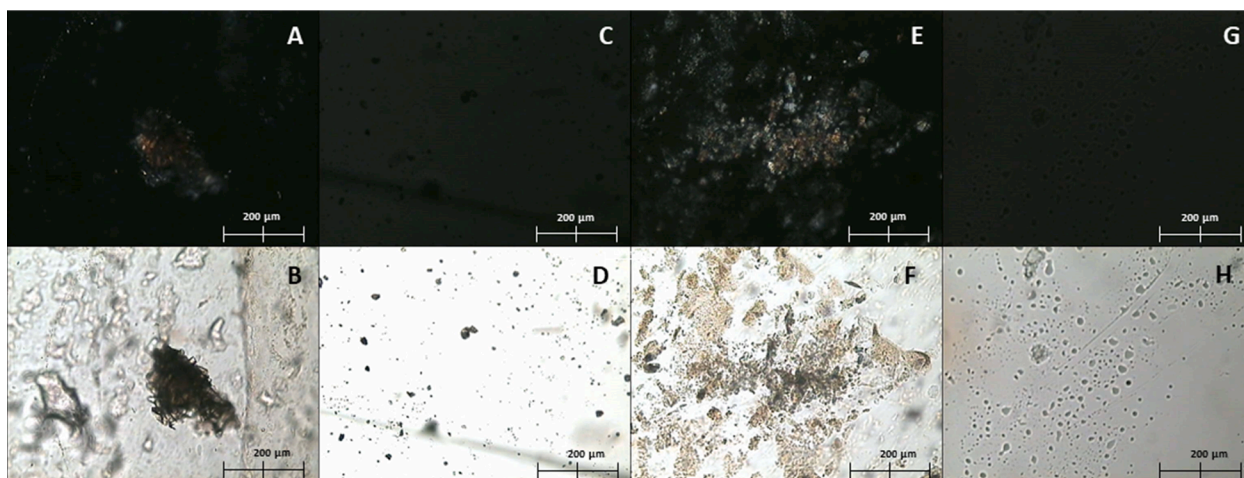


Fig. 10. HSPM of 3D printed implants: at 60°C of PCL_5PP_PM (A,B), PCL_5PP_CM (C, D), PCL_10PP_PM (E, F), PCL_10PP_CM (G, H). Upper pictures present the results with a polarized glass.

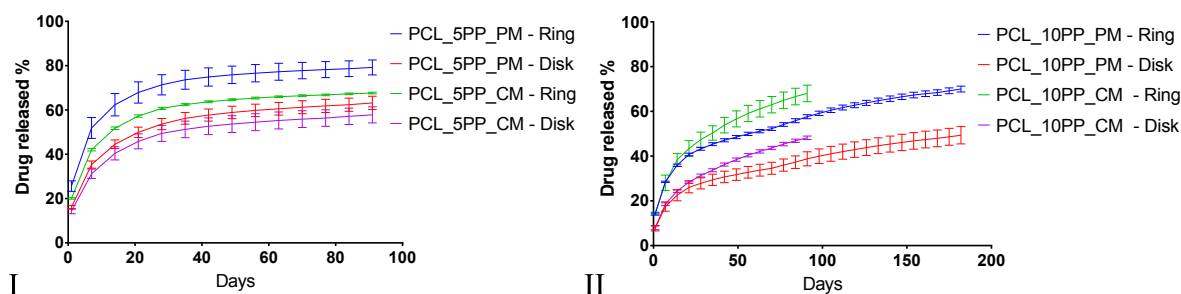


Fig. 11. Drug released (%) from 3D printed implants, from Blends PCL_5PP_PM, PCL_5PP_CM (I) and PCL_10PP_PM, PCL_10PP_CM (II) ($n = 3$).

the third week. Afterwards, a noticeable difference was observed and the implants that were printed from PCL_10PP_CM released a higher percentage of PP. After 3 months, PCL_10PP_PM released $57.6 \pm 0.9\%$ and $38.8 \pm 3.2\%$ of PP from the rings and disks, respectively. At the same time, PCL_10PP_CM, containing the amorphous form of PP, released $68 \pm 3.7\%$ and $48 \pm 0.8\%$ of drug from the rings and disks, respectively. It could be also noted that the dissolution curves of PP from the rings and disks that were printed with PCL_10PP_PM showed a bimodal release. The first phase started from day one and ended with a slower release after 2 months. After 70 days, a new phase started, which corresponded to an acceleration of the release of PP. The dosage forms containing the amorphous PP (PCL_10PP_CM) did not show this two-phase release. In this case, the design of the dosage forms as well as the preparation method had an impact on the release profile of PP.

A difference in terms of percentage of drug released was highlighted in comparison with the results observed in Fig. 11, I. Indeed, PCL_10PP_PM & PCL_10PP_CM, released the same percentage of PP after 1 day, which was not the case with PCL_5PP_PM & PCL_5PP_CM. In addition to this, PCL_10PP_CM, released a higher percentage of drug with time. At the end of 3 months, the dissolution test continued for PCL_10PP_PM to reach the same percentage released as PCL_10PP_CM. It took 180 days for the rings and disks printed from PCL_10PP_PM to release an equivalent amount of drug than PCL_10PP_CM after 3 months. However, here again, from the release profiles of the rings and disks printed from PCL_10PP_PM & PCL_10PP_CM, the ring shape implant have released the highest percentage of PP.

The impact of design on drug delivery has already been highlighted in the literature. Indeed, 3D printing allows a large versatility in terms of internal and external design. These parameters might have an impact on the amount of drug that may be released from the 3D printed dosage form. Goyanes et al., have printed tablets of paracetamol with different geometries, such as cubes, cylinders, torus, pyramids and a sphere. They have shown that the higher the surface/volume ratio, the higher the amount of drug released (Goyanes et al., 2015). In our case, the same results could be observed, independently of the preparation way, the rings have released more PP than disks. Moreover, it was also demonstrated that the rings have released the drug faster than the disks.

However, blends loaded with 10% w/w of PP released the drug less quickly than those loaded with 5% w/w of PP. This effect has already been observed several times in the literature, in articles on drugs-loaded PCL. For example, Hollander et al observed the same effect with an intrauterine system based on indomethacin-loaded PCL prepared by Fused deposition modeling (Holländer et al., 2016). Wang et al, observed the same results with hollow core fibers of polycaprolactone loaded with different amount of ketoconazole by coaxial electrospinning (Wang et al., 2016). Rychter et al, worked on cilostazol-loaded polycaprolactone by electrospinning and observed a decrease in drug release with higher drug-loaded formulations (Rychter et al., 2018). It can be observed that this phenomenon was repeated when BCS class II drugs were loaded in PCL. This class of drugs concerns molecules with a low aqueous solubility and high permeability (Tsume et al., 2014). Several hypotheses can explain this slower release when the amount of the loaded drug

increases.

A higher quantity of drugs may be present at the surface of the implant (Rychter et al., 2018). Increasing the amount of drugs, increases the hydrophobicity of the system and slow down the diffusion of water into the dosage form. Another hypothesis would be an increase in drug-drug interactions within the system which may lead to decrease their diffusion/release through the matrix (Wang et al., 2016). Finally, more drugs could be entrapped in the crystalline regions of the polymer, making it more difficult for water to diffuse into these regions which slow down the release of the drug (Rychter et al., 2018).

In addition, according to the results obtained from the dissolution tests, it was observed that the release of PP from the 3D printed dosage forms was never completed. Drug remained inside the implants after 3 or even 6 months. Since PCL is known to be used as a polymer to reach long-term drug release, two well-known mechanisms are described to allow this prolonged drug release. They are both based on the degradation/erosion of the polymer and diffusion of the drug through the polymer matrix (Repanas and Glasmacher, 2015). Several factors interact with these mechanisms, such as the molecular weight of the polymer and that of the loaded drug. Navitha et al. have made implants by Hot-Melt extrusion of risperidone-loaded PCL. They have shown that the use of PCL derivatives characterized by different molecular weights could modulate the dissolution profile of risperidone (Navitha and Jogala, 2014).

For their part, Potrč et al, compared the drug release of ibuprofen and carvedilol-loaded PCL nanofibers which were prepared by electrospinning. The results of the *in vitro* dissolution tests showed that the nanofibers loaded with ibuprofen released the drug faster than those loaded with carvedilol. This observation was independent of the drug crystallinity or nanofibers morphology. Therefore such result could be explained by the molecular weight of ibuprofen, which was half that of carvedilol, facilitating the diffusion of the drug that was characterized by the lowest molecular weight (Potrč et al., 2015).

In order to understand the release of PP from the 3D printed dosage forms with time, two evaluations were made. The first evaluation focused on the decrease in molecular weight (M_w) of PCL at different times during the dissolution test (Fig. 12A). The second evaluation concerned the measurement of the contact angle to evaluate the impact of hydrophobicity of PP on the blends (Fig. 12B). Indeed, as an increase of its concentration led to a decrease of its release, it was relevant to evaluate the potential effect of its presence at the surface of the 3D printed dosage forms, which was supposed to increase the global hydrophobicity of the implants, on its own release.

As it can be observed, the mean M_w values of PCL after 1 day of dissolution were $94,900 \pm 600$, $95,200 \pm 100$, $95,800 \pm 700$ and $98,600 \pm 2100$ g/mol for PCL_5PP_PM, PCL_5PP_CM, PCL_10PP_PM and PCL_10PP_CM, respectively (Fig. 12A). After 90 days, an average loss of $18.3 \pm 0.8\%$ was observed of the initial M_w for all blends. These results indicate that PCL derivative slowly degraded and/or eroded over time. This effect is partly responsible for the release of the drug, which may explain the very slow release of the drug with time. Nevertheless, the loss in mass is homogeneous for all blends, which does not explain why

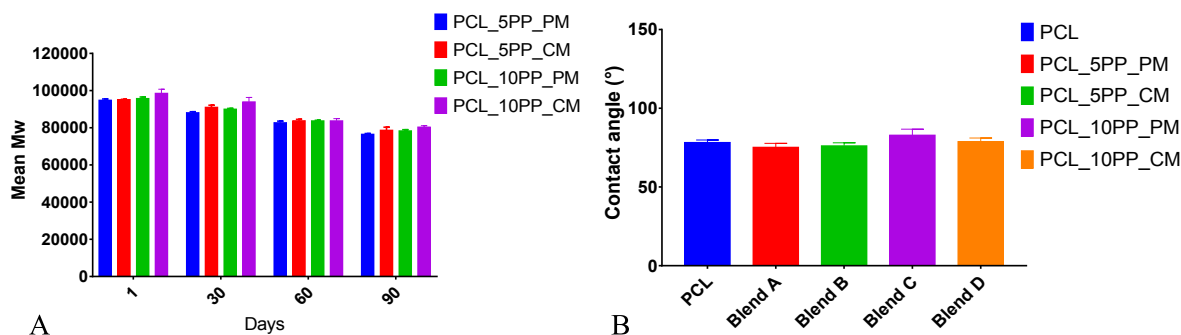


Fig. 12. (A) Mean Mw of PCL measured by GPC after different 1, 30, 60 and 90 Days, (B) contact angle measured on 3D printed implants.

blends containing 5% w/w PP release faster than formulations containing 10% w/w PP.

The contact angle measured were $78.3 \pm 1.6^\circ$, $75.2 \pm 2.5^\circ$, $76.2 \pm 1.9^\circ$, $82.9 \pm 3.8^\circ$ and $78.9 \pm 2.3^\circ$, respectively for PCL alone and PCL_5PP_PM, PCL_5PP_CM, PCL_10PP_PM and PCL_10PP_CM (Fig. 12B). The angles measured for PCL_5PP_PM & PCL_5PP_CM containing 5% w/w of PP are slightly lower than those obtained for PCL alone. On the other hand, the values observed for PCL_10PP_PM & PCL_10PP_CM loaded with 10% w/w of PP are slightly higher than the polymer alone. However, these results did not show large differences between the blends. Even if PCL_10PP_PM, containing 10% PP, which had the highest contact angle value, has shown the slowest drug release, the contact angles could not be used to explain the mechanism of drug release.

Nevertheless, the release of PP from a polymeric matrix such as PCL remains a complex phenomenon as it is the result of a combination of factors.

4. Conclusion

In conclusion, 3D printing by PEBP has shown to be an interesting alternative when the preparation of a printable filament is not possible. Using this technique, it has been possible to highlight the versatility of 3D printing in design by creating 3D printed dosage forms with different shapes. Indeed, during the *in vitro* dissolution test, the release profile of the PP has been modulated according to the shape of the implants. It was also possible to observe that cryogenic milling allowed the preparation of amorphous PP and the state was maintained after 3D printing. When the blends contained 10% w/w of PP, the amorphous form of the drug, in addition to the design, had an impact on the amount of drug that was released overtime. Long-acting implantable devices proved to be an interesting alternative form to improve compliance of patients suffering from schizophrenia. Also, the tunability obtained by PEBP allowed the obtention of different release profiles from a single formulation. However, the understanding of the phenomena leading to the release of PP has yet to be elucidated with additional analyses such as solid-state NMR, x-ray computed tomography or Raman spectroscopy along the different stages of the dissolution test. Further studies need to be carried out to better predict the release of PP according to the design used, and to best meet the needs of patients.

CRedit authorship contribution statement

Giuseppe Manini: Investigation, Formal analysis, Writing - original draft. **Maud Deldime:** Investigation. **Samira Benali:** Writing - review & editing. **Jean-Marie Raquez:** Supervision, Validation, Writing - review & editing. **Jonathan Goole:** Supervision, Validation, Writing - review & editing.

Declaration of Competing Interest

The authors declare that they have no known competing financial

interests or personal relationships that could have appeared to influence the work reported in this paper.

Acknowledgements

Giuseppe Manini was supported by the Belgian Fund for Research training in Industry and Agriculture for its financial support (FRIA grant). S. Benali thanks the special supports by the European Community (FEDER) in the frame of LCFM-BIOMAT and Interreg France-Wallonie-Vlaanderen program, 3D4Med. J.M. Raquez is Chercheur Qualifié from Belgian FNRS agency.

References

- Aho, J., Natalja, G., Magnus, E., Johan, B., Stefania, B., Jukka, R., 2016. Drug-loaded poly(ϵ -caprolactone) for 3D printing of personalized medicine: A difference during polymer melt extrusion flows rheological study. *Annu. Trans. Nord Rheol. Soc.* 24.
- Aho, J., Bøtker, J.P., Genina, N., Edinger, M., Arnfast, L., 2019. Roadmap to 3D-printed oral pharmaceutical dosage forms: feedstock filament properties and characterization for fused deposition modeling. *J. Pharm. Sci.* 108 (1), 26–35. <https://doi.org/10.1016/j.xphs.2018.11.012>.
- Azad, M.A., Olawuni, D., Kimbell, G., Badruddoza, A.Z., Hossain, S., Sultana, T., 2020. Polymers for extrusion-based 3D printing of pharmaceuticals: a holistic materials – process perspective. *Pharmaceutics* 1–34.
- Cader, H.K., Rance, G.A., Alexander, M.R., et al., 2019. Water-based 3D inkjet printing of an oral pharmaceutical dosage form. *Int. J. Pharm.* 564 (April), 359–368. <https://doi.org/10.1016/j.ijpharm.2019.04.026>.
- Cheng, L., Guo, S., Wu, W., 2009. Characterization and *in vitro* release of praziquantel from poly(ϵ -caprolactone) implants. *Int. J. Pharm.* 377 (1–2), 112–119. <https://doi.org/10.1016/j.ijpharm.2009.05.007>.
- Darville, N., Heerden, V., Marjolein Vynckier, A., De Meulder, M., Sterkens, P., Annaert, P., Van Den Mooter, G., 2014. Intramuscular administration of paliperidone palmitate extended-release injectable microsuspension induces a subclinical inflammatory reaction modulating the pharmacokinetics in rats. *Pharm. Drug Deliv. Pharm. Technol.* <https://doi.org/10.1002/jps.24014>.
- Dissolution Methods Database | FDA. <https://www.fda.gov/drugs/drug-approvals-and-databases/dissolution-methods-database>. Accessed January 29, 2021.
- El Aita, I., Bretkreutz, J., Quodbach, J., 2019. On-demand manufacturing of immediate release levetiracetam tablets using pressure-assisted microsyringe printing. *Eur. J. Pharm. Biopharm.* 134, 29–36. <https://doi.org/10.1016/j.ejpb.2018.11.008>.
- Elmowafy, M., Alruwaili, N.K., Shalaby, K., et al., 2020. Long-acting paliperidone parenteral formulations based on polycaprolactone nanoparticles; the influence of stabilizer and chitosan on *in vitro* release, protein adsorption, and cytotoxicity. *Pharmaceutics*.
- Fina, F., Goyanes, A., Gaisford, S., Basit, A.W., 2017. Selective laser sintering (SLS) 3D printing of medicines. *Int. J. Pharm.* 529 (1–2), 285–293. <https://doi.org/10.1016/j.ijpharm.2017.06.082>.
- Fina, F., Goyanes, A., Madla, C.M., et al., 2018. 3D printing of drug-loaded gyroid lattices using selective laser sintering. *Int. J. Pharm.* 547 (1–2), 44–52. <https://doi.org/10.1016/j.ijpharm.2018.05.044>.
- Goyanes, A., Martinez, P.R., Buanz, A., Basit, A.W., Gaisford, S., 2015;(July):1–8. Effect of geometry on drug release from 3D printed tablets. *Int. J. Pharm.* <https://doi.org/10.1016/j.ijpharm.2015.04.069>.
- Goyanes, A., Allahham, N., Tren, S.J., Stoyanov, E., Gaisford, S., Basit, A.W., 2019. Direct powder extrusion 3D printing: Fabrication of drug products using a novel single-step process. 567 (May) <https://doi.org/10.1016/j.ijpharm.2019.118471>.
- Holländer, J., Genina, N., Jukarainen, H., et al., 2016. Three-dimensional printed PCL-based implantable prototypes of medical devices for controlled drug delivery. *J. Pharm. Sci.* 105 <https://doi.org/10.1016/j.xphs.2015.12.012>.
- Huang, S., Donnell, K.P.O., De, V.S.M.D., Brien, J.O., Stutzman, J., Iii, R.O.W., 2017. Processing thermally labile drugs by hot-melt extrusion: the lesson with gliclazide. *Eur. J. Pharm. Biopharm.* <https://doi.org/10.1016/j.ejpb.2017.05.014>.

- Infanger, S., Haemmerli, A., Iliev, S., Baier, A., Stoyanov, E., Quodbach, J., August 2018. Powder bed 3D-printing of highly loaded drug delivery devices with hydroxypropyl cellulose as solid binder. *Int. J. Pharm.* 2019 (555), 198–206. <https://doi.org/10.1016/j.ijpharm.2018.11.048>.
- Jiao, Z., Luo, B., Xiang, S., Ma, H., Yu, Y., Yang, W., 2019. Polymer research 3D printing of HA / PCL composite tissue engineering scaffolds. *Adv. Ind. Eng. Polym. Res.* 2 (4), 196–202. <https://doi.org/10.1016/j.aiepr.2019.09.003>.
- Jonathan, G., Karim, A., 2015. 3D printing in pharmaceuticals: A new tool for designing customized drug delivery systems. *Int. J. Pharmaceutics*. <https://doi.org/10.1016/j.ijpharm.2015.12.071>.
- Kempin, W., Franz, C., Koster, L., et al., 2017. Assessment of different polymers and drug loads for fused deposition modeling of drug loaded implants. *Eur. J. Pharm. Biopharm.* <https://doi.org/10.1016/j.ejpb.2017.02.014>.
- Khaled, S.A., Burley, J.C., Alexander, M.R., Yang, J., Roberts, C.J., 2015. 3D printing of five-in-one dose combination poly pill with de fined immediate and sustained release profiles. *J. Control. Release* 217, 308–314. <https://doi.org/10.1016/j.jconrel.2015.09.028>.
- Leng, D., Chen, H., Li, G., et al., 2014. Development and comparison of intramuscularly long-acting paliperidone palmitate nanosuspensions with different particle size. *Int. J. Pharm.* 380–385 <https://doi.org/10.1016/j.ijpharm.2014.05.052>.
- Li, C., Cheng, L., Zhang, Y., Guo, S., Wu, W., 2010. Effects of implant diameter, drug loading and end-capping on praziquantel release from PCL implants. *Int. J. Pharm.* 386 (1–2), 23–29. <https://doi.org/10.1016/j.ijpharm.2009.10.046>.
- Loh, Z.H., Samanta, A.K., Sia Heng, P.W., 2014. Overview of milling techniques for improving the solubility of poorly water-soluble drugs. *Asian J. Pharm. Sci.* 10 (4), 255–274. <https://doi.org/10.1016/j.ajps.2014.12.006>.
- Marsac, P.J., Li, T., Taylor, L.S., 2009. Estimation of drug – polymer miscibility and solubility in amorphous solid dispersions using experimentally determined interaction parameters. *Pharm. Res.* 26 (1), 40–44. <https://doi.org/10.1007/s11095-008-9721-1>.
- Martinez, P.R., Goyanes, A., Basit, A.W., Gaisford, S., 2017. Fabrication of drug-loaded hydrogels with stereolithographic 3D printing. *Int. J. Pharm.* 532 (1), 313–317. <https://doi.org/10.1016/j.ijpharm.2017.09.003>.
- Melocchi, A., Uboldi, M., Maroni, A., et al., 2020. 3D printing by fused deposition modeling of single- and multi-compartment hollow systems for oral delivery – A review. *Int. J. Pharm.* 579 (February), 119155 <https://doi.org/10.1016/j.ijpharm.2020.119155>.
- Navitha, A., Jogala, S., 2014. Development of novel risperidone implants using blends of polycaprolactones and in vitro in vivo correlation studies. 5 (2), 84–90. <https://doi.org/10.4103/2231-4040.133431>.
- Nober, C., Manini, G., Carlier, E., et al., 2019. Feasibility study into the potential use of fused-deposition modeling to manufacture 3D-printed enteric capsules in compounding pharmacies. *Int. J. Pharm.* 569 <https://doi.org/10.1016/j.ijpharm.2019.118581>.
- Park, S.Y., Choi, J.W., Park, J.K., et al., 2016. Tissue-engineered artificial oesophagus patch using three-dimensionally printed polycaprolactone with mesenchymal stem cells: A preliminary report. *Interact Cardiovasc Thorac Surg.* 22 (6), 712–717. <https://doi.org/10.1093/icvts/ivw048>.
- Pietrzak, K., Isreb, A., Alhnan, M.A., 2015. A flexible-dose dispenser for immediate and extended release 3D printed tablets. *Eur. J. Pharm. Biopharm.* 96 (August), 380–387. <https://doi.org/10.1016/j.ejpb.2015.07.027>.
- Potrč, T., Baumgartner, S., Roškar, R., et al., 2015. Electrospun polycaprolactone nanofibers as a potential oromucosal delivery system for poorly water-soluble drugs. *Eur. J. Pharm. Sci.* 75, 101–113. <https://doi.org/10.1016/j.ejps.2015.04.004>.
- Remenar, J.F., 2014. Making the leap from daily oral dosing to long-acting injectables: Lessons from the antipsychotics. *Mol. Pharm.* 11 (6), 1739–1749. <https://doi.org/10.1021/mp500070m>.
- Repanas, A., Glasmacher, B., 2015. Dipyridamole embedded in Polycaprolactone fibers prepared by coaxial electrospinning as a novel drug delivery system. *J. Drug Deliv. Sci. Technol.* 29, 132–142. <https://doi.org/10.1016/j.jddst.2015.07.001>.
- Rychter, M., Baranowska-Korczyn, A., Milanowski, B., et al., 2018. Cilostazol-loaded poly (ε-caprolactone) electrospun drug delivery system for cardiovascular applications. *Pharm. Res.* 35 (2) <https://doi.org/10.1007/s11095-017-2314-0>.
- Sandler, N., Määttä, A., Ihalainen, P., et al., 2011. Inkjet printing of drug substances and use of porous substrates-towards individualized dosing. *J. Pharm. Sci.* 100 (8) <https://doi.org/10.1002/jps>.
- Sun, H., Mei, L., Song, C., Cui, X., Wang, P., 2006. The in vivo degradation, absorption and excretion of PCL-based implant. *Biomaterials* 27, 1735–1740. <https://doi.org/10.1016/j.biomaterials.2005.09.019>.
- Trivedi, R.K., Jain, P., Patel, M.C., Chatrabhuji, P.M., Trivedi, D.R., 2013. A Rapid. Stability Indicating RP-UPLC Method for Determination of Paliperidone Palmitate in a Depot Injectable Formulation. 3 (07), 87–92. <https://doi.org/10.7324/JAPS.2013.3716>.
- Tsume, Y., Mudie, D.M., Langguth, P., Amidon, G.E., Amidon, G.L., 2014. The Biopharmaceutics Classification System: Subclasses for in vivo predictive dissolution (IPD) methodology and IVIVC. *Eur. J. Pharm. Sci.* 23 (1), 1–7. <https://doi.org/10.1016/j.ejps.2014.01.009>.
- Wang, B., Zheng, H., Chang, M.W., Ahmad, Z., Li, J.S., 2016. Hollow polycaprolactone composite fibers for controlled magnetic responsive antifungal drug release. *Colloids Surf. B Biointerfaces* 145, 757–767. <https://doi.org/10.1016/j.colsurfb.2016.05.092>.
- Xu, X., Robles-Martinez, P., Madla, C.M., et al., December 2019. Stereolithography (SLA) 3D printing of an antihypertensive polyprintlet: Case study of an unexpected photopolymer-drug reaction. *Addit. Manuf.* 2020 (33), 101071 <https://doi.org/10.1016/j.addma.2020.101071>.
- Yang, G.H., Lee, H., Kim, G.H., 2018. Preparation and characterization of spiral-like micro-struts with nano-roughened surface for enhancing the proliferation and differentiation of preosteoblasts. *J. Ind. Eng. Chem.* 61, 244–254. <https://doi.org/10.1016/j.jiec.2017.12.022>.
- Yerragunta, B., Jogala, S., Chinnala, K.M., Aukunuru, J., 2015. Development of a novel 3-month drug releasing risperidone microspheres. *J. Pharm. Bioallied Sci.* 7 (1), 37–44. <https://doi.org/10.4103/0975-7406.148777>.